Binding of a potent small-molecule inhibitor of six-helix bundle formation requires interactions with both heptad-repeats of the RSV fusion protein

Dirk Roymans[a,1], Hendrik L. De Bondt[a], Eric Arnoult[b], Peggy Geluykens[a], Tom Gevers[c], Marcia Van Ginderen[a], Nick Verheyen[a], Hidong Kim[d], Rudy Willebrords[e], Jean-François Bonfanti[b], Wouter Bruinzeel[e], Maxwell D. Cummings[a], Herman van Vlijmen[a], and Koen Andries[e]

[a]Tibotec BVBA, B-2800 Mechelen, Belgium; [b]Tibotec, a division of Janssen-Cilag, Campus de Maigremont-BP615, F-27106 Val de Reuil Cedex, France; [c]Tibotec BVBA Turnhoutseweg 30, B-2340 Beerse, Belgium; [d]deCODE biostructures Inc, Bainbridge Island, WA 98110; and [e]Johnson & Johnson Pharmaceutical Research and Development, Turnhoutseweg 30, B-2340 Beerse, Belgium

Edited by Robert A. Lamb, Northwestern University, Evanston, IL, and approved November 4, 2009 (received for review September 4, 2009)

Six-helix bundle (6HB) formation is an essential step for many viruses that rely on a class I fusion protein to enter a target cell and initiate replication. Because the binding modes of small molecule inhibitors of 6HB formation are largely unknown, precisely how they disrupt 6HB formation remains unclear, and structure-based design of improved inhibitors is thus seriously hampered. Here we present the high resolution crystal structure of TMC353121, a potent inhibitor of respiratory syncytial virus (RSV), bound at a hydrophobic pocket of the 6HB formed by amino acid residues from both HR1 and HR2 heptad-repeats. Binding of TMC353121 stabilizes the interaction of HR1 and HR2 in an alternate conformation of the 6HB, in which direct binding interactions are formed between TMC353121 and both HR1 and HR2. Rather than completely preventing 6HB formation, our data indicate that TMC353121 inhibits fusion by causing a local disturbance of the natural 6HB conformation.

cocrystal structure | respiratory syncytial virus | TMC353121 | viral fusion

To allow the deposition of their nucleic acid genome into a host cell, and to initiate their replication cycle, enveloped viruses have evolved complex membrane fusion machinery that includes a fusion protein (1, 2). Based on structural similarity, the viral fusion proteins from different viruses have been grouped into three distinct classes: I, II, and III (3, 4). Prototypic trimeric class I fusion proteins include HIV-1 gp41, influenza hemagglutinin and the fusion proteins from paramyxoviruses. The fusion protein (F) of respiratory syncytial virus (RSV), a paramyxovirus belonging to the pneumovirinae subfamily, assembles into a homotrimer that is cleaved at two proximal furin cleavage sites during biosynthesis, priming the protein for membrane fusion. Proteolytic cleavage of the fusion protein precursor (F_0) yields two polypeptides, F_1 and F_2, joined by a disulfide bridge (Fig. 1). F_1 consists of an N-terminal hydrophobic fusion peptide, followed by a first heptad-repeat (HR1), an intervening globular domain, and a second heptad-repeat (HR2), which itself is N-terminal to the viral transmembrane and cytoplasmic regions (3). Once fusion is triggered, dramatic refolding of the prefusion conformation of the viral fusion protein occurs. Functional and structural studies have provided evidence that a folding intermediate is formed that contains a coiled-coil structure of three HR1 heptad repeats (5–8). This intermediate allows the fusion peptide to be inserted into the plasma membrane of a target cell. In the final stage of membrane fusion, the HR1-CTC structure irreversibly refolds into a 6HB complex with three HR2 heptad-repeats, resulting in membrane merger and stable fusion pore formation (5–14). In many viruses that rely on class I fusion proteins, the central HR1 trimeric coiled-coil (HR1-CTC) contains a hydrophobic pocket in each of its three grooves that has been proposed as a potential drug binding site (9, 10).

The therapeutic value of inhibiting 6HB formation was established with the development of the anti-HIV oligopeptide enfuvirtide (Fuzeon; ref. 15). Since the emergence of Fuzeon, numerous efforts have been initiated to develop new peptides, cyclic D-peptides and small-molecules that inhibit fusion (16–38). Although it is well understood that peptides inhibit fusion by competitively preventing 6HB formation (21, 22, 39, 40), the various mechanisms by which small-molecules that target the HR1-CTC inhibit 6HB formation remain largely unclear. These small-molecule inhibitors are thought to bind to the three identical hydrophobic pockets of the HR1-CTC folding intermediate, competing with HR2 for this site and thus preventing or disturbing natural 6HB formation (24, 27–34). However, to date there has been no direct structural evidence to support this hypothesis.

We now show that TMC353121, a potent RSV fusion inhibitor, binds to the 6HB through interactions with both HR1 and HR2. Rather than completely preventing HR2 binding to the HR1-CTC, binding of TMC353121 induces an alternate nonhelical conformation of the N terminus of HR2 in the 6HB. The presented binding mode is fully consistent with the structure-activity relationship of the TMC353121 series of compounds.

Results

TMC353121 Inhibits Both Virus–Cell and Cell–Cell Fusion. In a previous study, we reported the discovery of a series of substituted benzimidazoles that act as RSV fusion inhibitors (24). To confirm the mechanism of action, we added TMC353121, a representative member of the benzimidazole chemical series (25, 26), to parallel cultures of HeLa/M cells at different pre- and postvirus exposure time points. We evaluated the ability of the compound to inhibit production of extracellular progeny virus and cytopathic effect (CPE) by syncytia formation in comparison with other described RSV 6HB inhibitors (Fig. 2*A*; ref. 24, 27, 28, 41). All compounds effectively inhibit RSV replication when added up to 3 h postvirus exposure (Fig. 2*B*), hence acting early in the viral replication cycle. In addition, the compounds could be added as late as 15 h

Author contributions: D.R., H.L.D.B., E.A., H.K., and J.-F.B. designed research; D.R., P.G., T. G., M.V.G., N.V., J.-F.B., and W.B. performed research; D.R., H.L.D.B., E.A., H.K., R.W., J.-F. B., M.D.C., H.V.V., and K.A. analyzed data; D.R. and M.D.C. wrote the paper.

The authors declare a conflict of interest. Some of the structural work, described in this manuscript, has been performed by decode Biostructures as contract research for Tibotec BVBA. All the authors, except Hidong Kim, are current employees of Tibotec BVBA (Johnson & Johnson).

This article is a PNAS Direct Submission.

Accession: The atomic coordinates and structure factors for the reported crystal structure have been deposited in the RSCB Protein Data Bank under PDB ID 3KPE.

Database deposition: Crystallography, atomic coordinates, and structure factors

[1]To whom correspondence should be addressed. E-mail: droymans@its.jnj.com.

This article contains supporting information online at www.pnas.org/cgi/content/full/0910108106/DCSupplemental

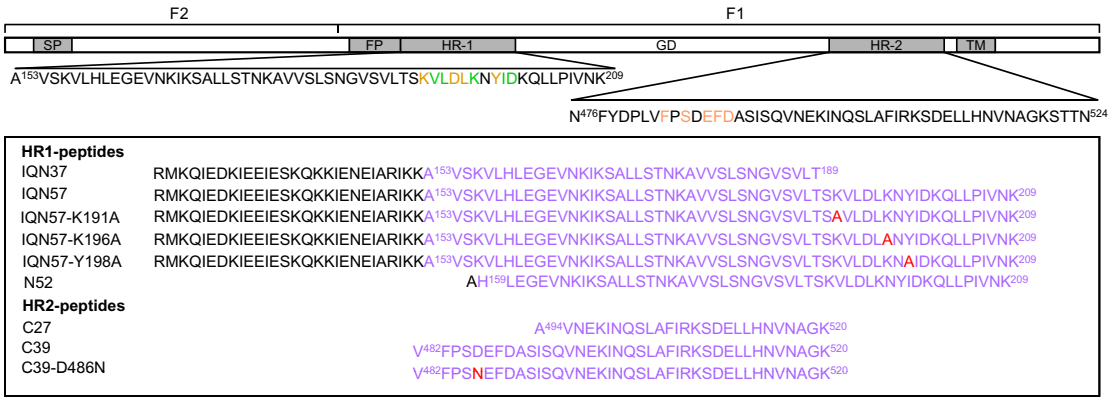

Fig. 1. Peptide sequences and mapping. Annotations, protein sequences, and mapping in the F_1 polypeptide of the peptides used in the different experiments. Black represents the IQ (=GCN4-$_{pI_Q}$I) part of the peptide, purple represents the HR1- or HR2-derived part, and red indicates the mutated positions. Numbers in superscript annotate the amino acid position in the full length F protein sequence of the A2 strain virus. Amino acids from two neighboring HR1 α-helices composing the HR1 hydrophobic pocket are indicated in ochre (HR1) and green (HR1′). HR2 amino acids that interact with the HR1 hydrophobic pocket are indicated in orange.

postinfection and still inhibit syncytia formation by 50% (Fig. 2*C*). These results suggest that TMC353121 inhibits both virus–cell and cell–cell fusion.

In Vitro Resistance Mutations Raised Against TMC353121 Are Located in the F Protein. We raised resistant mutants in vitro to confirm that TMC353121 targets the F protein. Stable but single S398L and D486N mutations were selected in both Long strain and rgRSV224 viruses. The latter virus also selected for the S398L mutation, which in this case was followed by the appearance of an additional K394R mutation. D486N results in a 2,474-fold increase in EC_{50}, while S398L causes a much more modest 194-fold increase. The EC_{50} of the K394R/S398L double mutant in rgRSV224 is increased more than 30,000-fold (taking the CC_{50} value of TMC353121 into account).

The observed mutations in response to TMC353121 are in the same F_1 polypeptide regions as those described previously for other small-molecule inhibitors of 6HB formation in RSV (24, 28, 42). K394R and S398L are in the cysteine-rich region of the globular loop domain, whereas D486N is in the HR2 region that interacts with the HR1 hydrophobic pockets in the 6HB. No mutations were observed in other proteins of the virus, suggesting that the F protein is the sole target of TMC353121.

TMC353121 Binding to F Requires Interactions with Both HR1 and HR2 Heptad Repeats. The above results, together with previous work from our laboratory (24–26) and others (28, 42), suggests that TMC353121 binds at the known hydrophobic pockets of the HR1-CTC. To further explore this hypothesis, we synthesized [^{125}I]TMC429962, a close and active analog of TMC353121 containing a diazirine moiety and an ^{125}I atom (Fig. 3*A*). The diazirine moiety allows the compound to be covalently coupled to its target site by irradiating it with long wave UV light (27, 43), although the ^{125}I atom serves as a radiotracer. This reagent allowed us to monitor the binding of [^{125}I]TMC429962 to peptides derived from HR1 and HR2 (Fig. 1).

N57 (HR1) and C39 (HR2) have previously been shown to constitute the proteinase K-resistant core of the RSV 6HB (10). IQN57 consists of N57 fused N-terminally to the trimeric coiled-coil GCN4-$_{pI_Q}$I (IQ) (44), which improves the solubility of N57. Fusion of both coiled-coils was designed to preserve the heptad-repeat structure of IQN57 (Fig. 1). [^{125}I]TMC429962 alone, or in combination with C39, was administered to a solution of IQN57.

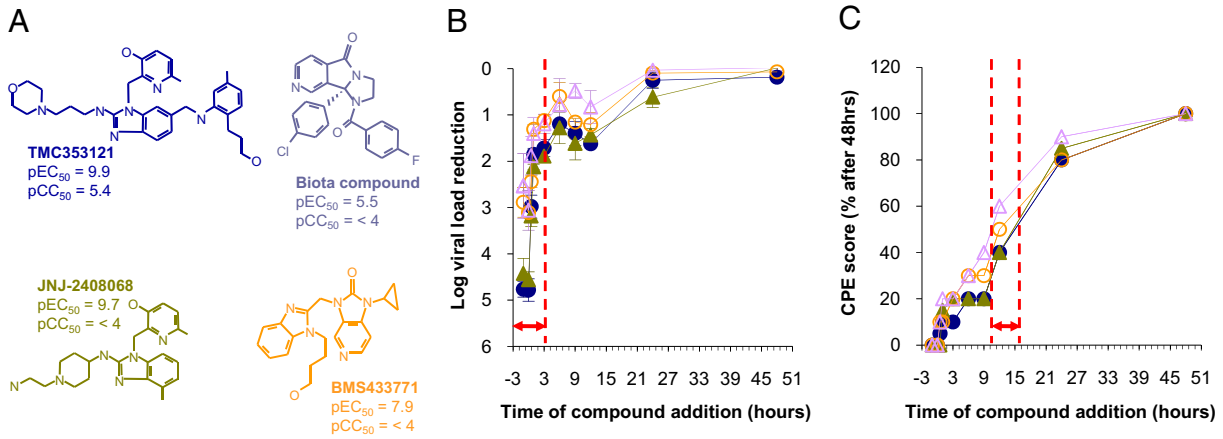

Fig. 2. Time of addition profiling of 6HB formation inhibitors. Structures of the fusion inhibitors, together with their in vitro anti-RSV activity [$pEC_{50} = -\log_{10} EC_{50}$ (M)] and cytotoxicity [$pCC_{50} = -\log_{10} CC_{50}$ (M)], that were included in the test panel (*A*). TMC353121 (blue full circles), JNJ-2408068 (green full triangles), and BMS433771 (orange open circles) at concentration 100 x EC_{50} [20 x EC_{50} for the Biota compound (purple open triangles)] were added in a time of addition experiment to the infected cells as indicated on the *x* axis. Time point −1 h represents a 1 h preincubation of compound and virus before infection. Red arrows indicate the period of the replication cycle in which the compounds are able to block viral replication as demonstrated by plaque assay (*B*) or to prevent 50% syncytium formation (*C*). Values are presented as the mean ± SEM in (*B*). (*C*) shows one representative result of three independent experiments.

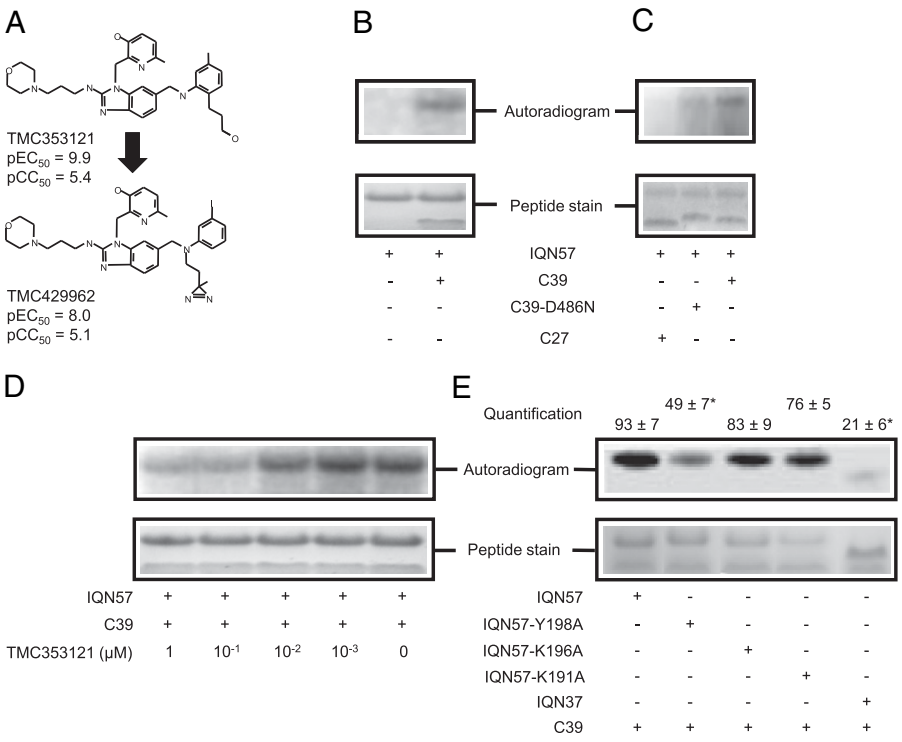

Fig. 3. Photoaffinity labeling with [^{125}I]TMC429962. Structures of TMC353121 and TMC429962 are presented, together with their in vitro anti-RSV activity [$pEC_{50} = -\log_{10} EC_{50}$ (M)] and cytotoxicity [$pCC_{50} = -\log_{10} CC_{50}$ (M)] (*A*). 10 nM [^{125}I]TMC429962 was incubated with 25 μM peptide solutions as indicated in the figures, irradiated with long wave UV light, electrophoresed and binding of [^{125}I]TMC429962 detected by autoradiography. Binding to WT HR1- and HR2-derived peptides (*B*). Binding to mutant HR2-derived peptides (*C*). Binding competition between 10 nM [^{125}I]TMC429962 and different concentrations of TMC353121 as indicated in the figure (*D*). Binding to mutant HR1-derived peptides (*E*). Densitometric quantification of [^{125}I]TMC429962 binding to wild type and mutant HR1 peptides is shown as % [* *P* value < 0.05 (mutant peptide versus wild type); *n* = 3].

Although [^{125}I]TMC429962 binds to IQN57 when C39 is present, binding cannot be detected in the absence of C39 (Fig. 3*B*). Reduced binding of [^{125}I]TMC429962 to IQN57 is observed with C39-D486N, a C39 peptide containing the D486N resistance mutation, and binding is also completely abrogated for C27, a deletion mutant of C39 lacking the amino acids known to occupy the HR1-CTC hydrophobic pockets in the native 6HB (Figs. 1 and 3*C*). As expected, TMC353121 and [^{125}I]TMC429962 compete for the same binding pocket (Fig. 3*D*).

To identify HR1 residues critical for binding of TMC353121, single alanine mutants of IQN57 at positions K191, K196, and Y198 were synthesized (Fig. 1), based on computer assisted prediction of electrostatic interactions between the side chains of these amino acids and TMC353121. Binding of [^{125}I]TMC429962 to the IQN57-Y198A mutant is significantly reduced by approximately 50% (Fig. 3*E*), although little reduction of [^{125}I]TMC429962 binding is observed for K191A and K196A. [^{125}I]TMC429962 does not bind to IQN37, an IQN57 variant from which the HR1 hydrophobic pocket region is deleted (Fig. 1), confirming that [^{125}I]TMC429962 binds specifically to the hydrophobic pocket region of HR1 that includes Y198.

Altogether these data identify the region where TMC353121 binds, and demonstrate that interactions with amino acids from both HR1 (Y198) and HR2 (D486) play a crucial role in binding.

Cocrystal Structure of TMC353121 Bound to the 6HB Reveals an Alternate 6HB Conformation. To further understand the structural basis of the interaction of TMC353121 with both heptad repeats, we performed cocrystallization of TMC353121 with a 6HB construct. The construct consisted of an N52 peptide, derived from the sequence of HR1 including the HR1 hydrophobic pocket, and C39 (Fig. 1). This approach yielded crystals of the complex that diffracted to 1.47 Å resolution (Fig. S1). Bound TMC353121 fits unambiguously into the electron density maps.

The overall structure of the complex retains the threefold symmetry present in all published 6HB structures (Fig. 4*A*), and superimposes well with the previously reported apo RSV 6HB structure (PDB ID 1G2C; Ref. 10). TMC353121 binds at each of the three identical hydrophobic pockets of the trimeric HR1 core (Fig. 4*A*), and the electron density maps and refined *B*-factors indicate full occupancy and low disorder.

Binding of TMC353121 to the 6HB involves an induced fit in which the four N-terminal residues of C39 lose their helical conformation and no longer occupy the hydrophobic groove formed between neighboring HR1 helices. In the structure reported here this vacated site is now occupied by bound TMC353121, with the inhibitor sandwiched between the N52 and C39 peptides (Fig. 4*B*). The most significant conformational change involves a 136 degree rotation of the backbone ψ-angle of D486, resulting in partial unwinding of the α-helical backbone of HR2. In addition, the side chain conformations of HR1 residue D200 and HR2 residues D486 and E487 adopt different rotameric states to allow optimal interactions with bound TMC353121 (Table S1).

Bound TMC353121 makes several hydrophobic and electrostatic interactions with both the HR1 and HR2 components of the observed inhibitor binding site (Fig. 4*C*).The hydroxypyridine group is the most deeply buried part of the bound inhibitor and appears to make the most significant contribution to binding. This moiety is involved in multiple binding interactions with HR1: a hydrogen bond with the carboxylate of D200, parallel π–π stacking with Y198, and additional hydrophobic interactions with various residues of the binding site. The amino substituent at position 2 of the benzimidazole forms a hydrogen bond with D486 in HR2. Interestingly, F488, previously shown to occupy part of the HR1 hydrophobic pocket (10), is not significantly displaced when compared to the structure of the native RSV 6HB. Finally, a water-mediated hydrogen bonding network is observed between the side-chain of E487, the propanol hydroxyl, and the hydroxypyridine nitrogen of TMC353121. A polyethylene glycol molecule is observed bound near the morpholino group of TMC353121 (Fig. S2), but this does not appear to significantly impact the binding mode of TMC353121 (*SI Text*).

The TMC353121-bound complex buries 17% more surface area than the apo structure (5982 Å^2 and 5134 Å^2, respectively).

The Binding Mode of TMC353121 Is Fully Consistent with the Structure-Activity Relationship Observed for the TMC353121 Series of Inhibitors. Removal of the hydroxypropyl group (Table 1) causes

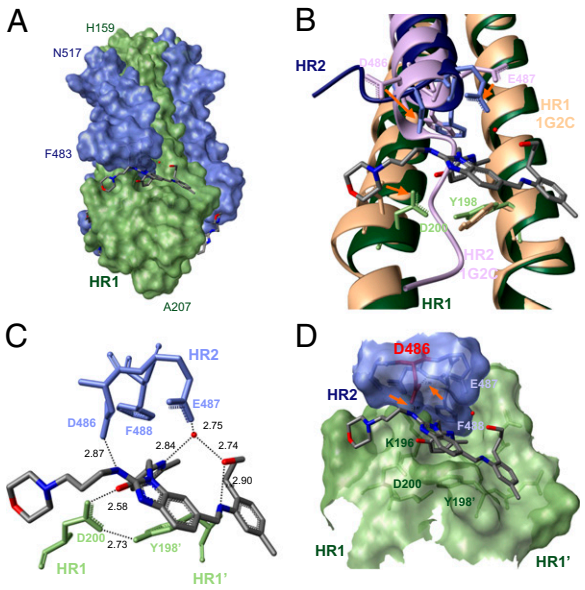

Fig. 4. Binding mode and interaction map of TMC353121 and effect of the D486N mutation on the interactions. Binding mode of TMC353121 in the complete 6HB (*A*). The RSV 6HB is composed of three central HR1 helices (green surface) surrounded by three antiparallel HR2 helices (blue surface). The 6HB axis is tilted approximately 45 degrees from the plane of the page. Superimposition of the TMC353121 cocrystal structure with the 1G2C RSV 6HB crystal structure (*B*). The HR1 and HR2 helices of the cocrystal structure are dark green and blue, respectively, and the HR1 and HR2 helices from the 1G2C 6HB structure are shown in salmon and lilac, respectively. Displacement of side-chains by TMC353121 is indicated by orange arrows. Interaction map of TMC353121 with its 6HB target site (*C*). H-bonds are drawn as black dotted lines. Distances (Å) between interacting atoms are in black. TMC353121 makes a π–π stacking interaction with Y198. Residues from two neighboring HR1 or HR1′ and HR2 helices are indicated in green and blue, respectively. Effect of the HR2 resistance mutation D486N on electrostatic interactions in the TMC353121-bound 6HB complex (D). HR1 or HR1′ and HR2 residues are indicated in dark green and blue, respectively, and the calculated protein surface of HR1 and HR2 in transparent green and blue, respectively. HR2 residue 486 that causes resistance against TMC353121 upon mutation is shown in red. Orange arrows indicate hydrogen bonds. TMC353121 is colored by atom type (carbon = gray; oxygen = red; nitrogen = blue).

a 1.3 log reduction in activity (compound 2), and further truncation of the methylaminotoluene moiety yields an additional 0.8 log decrease in potency (compound 3). These dramatic effects are likely due to unfavorable changes in the observed water-mediated hydrogen bonding network (Fig. 4*C*), and an overall reduction in hydrophobic binding contacts. The morpholinopropyl group is observed to slightly decrease the activity, as its removal gives a 0.6 log improvement in activity (compound 4). This is in agreement with the observed structure, as this moiety has virtually no direct interactions with the binding site. However, we note that this chemical group is incorporated for pharmacokinetic benefit (26). The amino substituent at position 2 of the benzimidazole is key; removal of this one moiety (compound 5) leads to a 2.6 log reduction in activity, highlighting the importance of the interaction with D486 (Fig. 4*C*). The importance of this contact is further established by the dramatic 3.4 log reduction in antiviral activity observed for TMC353121 against a virus bearing the D486N resistance-associated mutation. Finally, the observed interaction between the pyridine hydroxyl and D200 is consistent with the 1.3 log drop in activity observed for the methoxy analog (compound 6).

Binding of TMC353121 Stabilizes the 6HB. To understand the functional impact of the observed disturbance of natural 6HB formation by TMC353121, we investigated the influence of the compound on the stability of the 6HB. We used a thermal shift assay to measure the melting temperature (T_m) of both the apo and TMC353121-bound complexes and found that the T_m of the TMC353121-bound complex increases by 7 °C (58 ± 2 °C versus 51 ± 1 °C for N52/C39; $P < 0.025$). Thus, binding of TMC353121 stabilizes the 6HB. This qualitative indication of tight binding is consistent with the photo affinity labeling results, which implicate the involvement of both HR1 and HR2 in TMC353121 binding, as well as with the crystallographic result, which shows direct binding interactions between TMC353121 and both HR1 and HR2.

When the binding of a fixed concentration of FITC-labeled C39 (FITC-C39) to IQN57 was measured in a 6HB formation ELISA, we found that binding of FITC-C39 increases with increasing concentrations of TMC353121 (Fig. 5*A*, path 1; Fig. 5*B*), again consistent with the other observations that TMC353121 stabilizes the 6HB. In contrast, FITC-C39 binding is not enhanced when TMC353121 is incubated with IQN57 first and unbound compound is washed out before FITC-C39 administration (Fig. 5*A*, path 2; Fig. 5*B*). This again suggests that TMC353121 does not bind to the isolated HR1 hydrophobic pockets. Finally, when FITC-C39 is allowed to bind and form a 6HB with IQN57 prior to incubation with TMC353121, no influence on FITC-C39 binding is observed up to 30 min after compound administration (Fig. 5*A*, path 3; Fig. 5*B*). This result indicates that the binding of TMC353121 to a preformed 6HB is a slow process, and it is therefore unlikely that the activity of the compound can be attributed to events that occur after 6HB formation.

Discussion

The lack of structural information on the binding modes of small-molecule inhibitors of 6HB formation that target the HR1-CTC has limited our understanding of the mechanism of inhibition of these compounds and has restricted our ability to apply structure-based design techniques to drug discovery in this area. It is generally believed that these inhibitors bind to three identical hydrophobic pockets of the HR1-CTC (9, 10, 24, 27–34). However, several reported observations suggest that binding of high affinity members of such small-molecule inhibitors of 6HB may be more complex. First, small molecule inhibitors of HIV-1 6HB formation shown to prevent HR2 association and believed to bind to the HR1-CTC hydrophobic pockets all suffer from limited potency (29–32). Second, small organic building blocks covalently coupled to an HIV-1 HR2-derived sequence enhanced activity by 20-fold (33, 34), although the building blocks alone, which on the basis of the coupled sequences were predicted to occupy the HR1-CTC hydrophobic pockets, did not display any observable activity. Third, structural analysis of the HR1-CTC hydrophobic pockets by ourselves (26) and others (28) suggests that potent inhibition of fusion is unlikely to result solely from binding of compounds to the relatively small and shallow HR1 pockets. BMS433771, for example, a potent small molecule RSV fusion inhibitor shown to bind to the HR1 hydrophobic pockets, shows surprisingly weak binding affinity given its observed antiviral potency (27). Consideration of these observations, in conjunction with the binding mode observed for TMC353121, suggests that interactions with both heptad repeats may be a general requirement for high affinity binding of these small-molecule inhibitors of 6HB formation. This has implications for the discovery of new such inhibitors of 6HB formation in viruses that use class I fusion proteins, both in terms of structure-based design and assay development.

Our results demonstrate that, rather than completely preventing 6HB formation, binding of TMC353121 involves the formation of a distorted 6HB bundle, with TMC353121 sandwiched between HR1 and HR2 at the end of the 6HB distal to where the two fusing membranes are brought together. The complex structure also shows that the interaction of HR2 with the HR1-CTC, C-terminal to D486, is similar to that of the apo 6HB structure (10). This is

Table 1. TMC353121 structure-activity data. Structures of TMC353121 (compound 1) and analogs are shown together with their activity in an RSV cellular antiviral assay. In vitro activity is reported as pEC_{50}

TMC353121SAR

Compound	Structure	*In vitro* activity
1	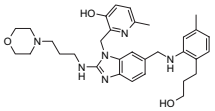	9.9
2	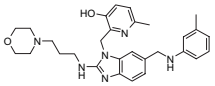	8.6
3	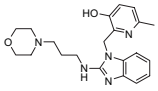	6.8
4	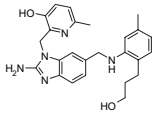	10.5
5	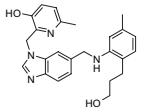	7.9
6	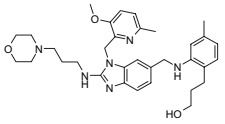	8.6

intriguing from a mechanistic point of view, because it may indicate that TMC353121 binding does not prevent the membranes from being apposed. The current model of paramyxoviral fusion predicts that the viral membrane is brought close to the host cell membrane by refolding of the fusion protein from a "prehairpin" to a "hairpin" conformation (1–8). In agreement with this model, in SV5 and HIV-1 it has been shown that membrane merger and stable pore formation are coupled directly to 6HB formation (7, 8), suggesting that the energy required for these late stage fusion events may come from 6HB formation. The mechanistic details of HR2 association with the HR1-CTC are currently not understood, and the possibility that the observed distorted 6HB in the presence of bound TMC353121 is an artifact of cocrystallizing the compound with separate HR1 and HR2 peptides instead of the full-length fusion protein cannot be excluded. However, if one envisions 6HB formation as the closing of a zipper beginning at the membrane proximal end and progressing toward the end at which the HR1 hydrophobic pockets are located, as suggested previously (28), a possible mechanism of inhibition can be derived from the observed TMC353121 binding mode. The presence of bound TMC353121 may disrupt the natural closing of the zipper by preventing interactions of (at least) the last four N-terminal HR2 residues with the HR1-CTC. Consistent with this proposal is the observation that these residues provide a major contribution to the stability of the 6HB, as shown by the 100,000-fold affinity decrease resulting from their deletion (Fig. S3); binding of TMC353121 increases the stability of the 6HB despite eliminating these crucial interactions of HR2 with the HR1-CTC. Interference with the terminal part of the zipping process may prevent the formation of a fusion-competent conformation of the fusion protein and/or may disturb the timing of 6HB formation required for stable pore formation. Complete delineation of the mechanistic details of this phenomenon requires further research. However, based on our current data, it appears that high affinity small-molecule inhibitors of 6HB formation act by stabilizing unnatural and nonproductive 6HB conformations rather than simply preventing 6HB formation.

The binding mode of TMC353121 provides a molecular explanation for the selection of the D486N resistance mutation. Because the sidechain of D486 forms a hydrogen bond with TMC353121 and an additional intramolecular hydrogen bond, D486N likely destabilizes the interaction with TMC353121, consistent with our observation of reduced binding of [^{125}I] TMC449962 to IQN57 with D486N-C39. Reduced affinity for TMC353121 is consistent with the reduction in susceptibility observed for the D486N mutant virus. The observed binding mode of TMC353121 does not explain the K394R and S398L mutations in the globular loop region. However, resistance mutations in fusion protein regions distinct from the binding site of fusion inhibitors have previously been described in RSV (24, 28, 42), as well as in other viruses including measles virus (45), arenavirus (37) or influenza A (38). In these viruses it has been demonstrated that these mutations alter the stability of the fusion protein to reestablish optimal viral fusion kinetics (37, 45 –47).

In summary, our results describe the binding mode of a small-molecule inhibitor of 6HB formation in RSV, extending our understanding of how viral fusion can be effectively inhibited. This information should fuel the discovery of other entry inhibitors targeting viruses that use class 1 fusion proteins.

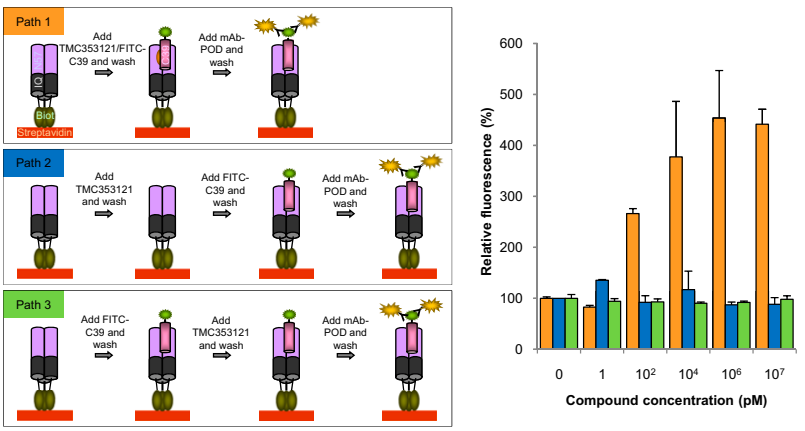

Fig. 5. Effect of TMC353121 on HR1/HR2-peptide interaction. Schematic representation of the different experimental conditions applied in the 6HB-ELISA (*A*). Influence of different concentrations of TMC353121 on the interaction between FITC-C39 with the HR1-CTC (*B*). The bars present tha data generated with three different experimental 6HB ELISA designs (orange = path 1; blue = path 2; green = path 3). Interaction between FITC-C39 and the HR1-CTC in the absence of TMC353121 was set at 100% (positive control), and the relative HR2 interaction with the HR1-CTC in the other conditions was normalized to this positive control condition. Values are from three independent experiments. *P* values and 95% confidence intervals are listed in Table S2.

Materials and Methods

6HB Complex Crystallization. N52 was produced by expressing the proteinase K resistant core of the HR1 region (10) as a fusion construct with Smt3 (50) and cleavage by a Ulp1 protease. C39 was chemically synthesized (Abgent). N52/C39 hexameric complex was prepared by mixing the C-peptide at a 1.1 molar excess with N52 solution yielding approximately 500 μM (15 mg/mL) N/C hexamers. TMC353121 was added to aliquots of the N52/C39 hexamer in a threefold molar excess to peptide binding sites. Crystallization was performed at room temperature by vapor diffusion. Equal volumes of N52/C39/TMC353121 solution and precipitant solution were combined. The structure was determined by molecular replacement using 1G2C as a search model (10). The ligand was unambiguously built into σ_A-weighted (51) F_{obs}–F_{calc} electron density maps.

Photoaffinity Labeling of Synthetic F_1 Peptides. Affinity labeling was performed by mixing 25 μM concentrations of peptide in binding buffer (PBS + 5% DMSO + 10% glycerol + an additional 100 mM NaCl) with 10 nM [^{125}I] TMC429962 (50 nM stock, 2000 Ci/mmol in methanol). Samples were irradiated for 15 min with long wave UV light (λ = 365 nm).

A detailed description of all experimental procedures is available in the *SI Materials and Methods*.

ACKNOWLEDGMENTS. The authors would like to thank M. Feese, E. Hansen, and J. Christensen for assistance in peptide preparation, crystallization, and x-ray diffraction data collection; B. Devogelaere, C. Liu, P. Branigan, J. Van Den Berg, P. Janssens, and H. Szel for technical assistance; L. Bijnens and R. Straetemans for performing statistical analyses. Prof. Y. Engelborghs and the members of its Laboratory of Biomolecular Dynamics (Katholic University of Leuven, Leuven, Belgium) for performing the CD experiments; J.K. Kranz for analyzing the thermal shift results and Luc Geeraert for editing the manuscript.

1. Colman PM, Lawrence MC (2003) The structural biology of type I viral membrane fusion. *Nat Rev Mol Cell Biol* 4:309–319.
2. Kielian M, Rey FA (2006) Virus membrane-fusion proteins: More than one way to make a hairpin. *Nat Rev Microbiol* 4:67–76.
3. Lamb RA, Jardetzky TS (2007) Structural basis of viral invasion: lessons from paramyxovirus F. *Curr Opin Struct Biol* 17:427–436.
4. Kadlec J, Loureiro S, Abrescia NG, Stuart DI, Jones IM (2008) The postfusion structure of baculovirus gp64 supports a unified view of viral fusion machines. *Nat Struct Mol Biol* 15:1024–1030.
5. Yin H-S, Paterson RG, Wen X, Lamb RA, Jardetzky TS (2005) Structure of the uncleaved ectodomain of the paramyxovirus (hPIV3) fusion protein. *Proc Natl Acad Sci USA* 102: 9288–9293.
6. Yin H-S, Wen X, Paterson RG, Lamb RA, Jardetzky TS (2006) Structure of the parainfluenza virus 5 F protein in its metastable, prefusion conformation. *Nature* 439: 38–44.
7. Melikyan GB, et al. (2000) Evidence that the transition of HIV-1 gp41 into a six-helix bundle, not the bundle configuration, induces membrane fusion. *J Cell Biol* 151: 413–423.
8. Russell CJ, Jardetzky TS, Lamb RA (2001) Membrane fusion machines of paramyxoviruses: capture of intermediates of fusion. *EMBO J* 20:4024–4034.
9. Chan DC, Chutkowski CT, Kim PS (1998) Evidence that a prominent cavity in the coiled coil of HIV type 1 gp41 is an attractive drug target. *Proc Natl Acad Sci USA* 95: 15613–15617.
10. Zhao X, Singh M, Malashkevich VN, Kim PS (2000) Structural characterization of the human respiratory syncytial virus fusion protein core. *Proc Natl Acad Sci USA* 97: 14172–14177.
11. Bullough PA, Hughson FM, Skehel JJ, Wiley DC (1994) Structure of influenza haemagglutinin at the pH of membrane fusion. *Nature* 371:37–43.
12. Malashkevich VN, Singh M, Kim PS (2001) The trimer-of-hairpins motif in membrane fusion: Visna virus. *Proc Natl Acad Sci USA* 98:8502–8506.
13. Supekar VM, et al. (2004) Structure of a proteolytically resistant core from the severe acute respiratory syndrome coronavirus S2 fusion protein. *Proc Natl Acad Sci USA* 101: 17958–17963.
14. Weissenhorn W, Carfí A, Lee KH, Skehel JJ, Wiley DC (1998) Crystal structure of the Ebola virus membrane fusion subunit, GP2, from the envelope glycoprotein ectodomain. *Mol Cell* 2:605–616.
15. Kilby JM, et al. (1998) Potent suppression of HIV-1 replication in humans by T-20, a peptide inhibitor of gp41-mediated virus entry. *Nat Med* 4:1302–1307.
16. Lambert DM, et al. (1996) Peptides from conserved regions of paramyxovirus fusion (F) proteins are potent inhibitors of viral fusion. *Proc Natl Acad Sci USA* 93:2186–2191.
17. Miller SA, Tollefson S, Crowe JE Jr, Williams JV, Wright DW (2007) Examination of a fusogenic hexameric core from human metapneumovirus and identification of a potent synthetic peptide inhibitor from the heptad repeat 1 region. *J Virol* 81: 141–149.
18. Bossart KN, et al. (2005) Inhibition of Henipavirus fusion and infection by heptad-derived peptides of the Nipah virus fusion glycoprotein. *Virol J* 2:57.
19. Rapaport D, Ovadia M, Shai Y (1995) A synthetic peptide corresponding to a conserved heptad repeat domain is a potent inhibitor of Sendai virus-cell fusion: an emerging similarity with functional domains of other viruses. *EMBO J* 14:5524–5531.
20. Bosch BJ, et al. (2004) Severe acute respiratory syndrome coronavirus (SARS-CoV) infection inhibition using spike protein heptad repeat-derived peptides. *Proc Natl Acad Sci USA* 101:8455–8460.
21. Eckert DM, Malashkevich VN, Hong LH, Carr PA, Kim PS (1999) Inhibiting HIV-1 entry: Discovery of D-peptide inhibitors that target the gp41 coiled-coil pocket. *Cell* 99: 103–115.
22. Welch BD, VanDemark AP, Heroux A, Hill CP, Kay MS (2007) Potent D-peptide inhibitors of HIV-1 entry. *Proc Natl Acad Sci USA* 104:16828–16833.
23. Debnath AK (2006) Prospects and strategies for the discovery and development of small-molecule inhibitors of six-helix bundle formation in class 1 viral fusion proteins. *Curr Opin Investig Drugs* 7:118–127.
24. Andries K, et al. (2003) Substituted benzimidazoles with nanomolar activity against respiratory syncytial virus. *Antiviral Res* 60:209–219.
25. Bonfanti J-F, et al. (2007) Selection of a respiratory syncytial virus fusion inhibitor clinical candidate, part 1: Improving the pharmacokinetic profile using the structure-property relationship. *J Med Chem* 50:4572–4584.
26. Bonfanti J-F, et al. (2008) Selection of a respiratory syncytial virus fusion inhibitor clinical candidate. 2. Discovery of a morpholinopropylaminobenzimidazole derivative (TMC353121). *J Med Chem* 51:875–896.
27. Cianci C, et al. (2004) Targeting a binding pocket within the trimer-of-hairpins: Small-molecule inhibition of viral fusion. *Proc Natl Acad Sci USA* 101:15046–15051.
28. Douglas JL, et al. (2005) Small molecules VP-14637 and JNJ-2408068 inhibit respiratory syncytial virus fusion by similar mechanisms. *Antimicrob Agents Chemother* 49:2460–2466.
29. Ernst JT, et al. (2002) Design of a protein surface antagonist based on alpha-helix mimicry: Inhibition of gp41 assembly and viral fusion. *Angew Chem Int Ed Engl* 41:278–281.
30. Jiang S, Debnath AK (2000) A salt bridge between an N-terminal coiled coil of gp41 and an antiviral agent targeted to the gp41 core is important for anti-HIV-1 activity. *Biochem Biophys Res Commun* 270:153–157.
31. Jiang S, et al. (2004) N-substituted pyrrole derivatives as novel human immunodeficiency virus type 1 entry inhibitors that interfere with the gp41 six-helix bundle formation and block virus fusion. *Antimicrob Agents Chemother* 48: 4349–4359.
32. Liu S, et al. (2005) Theaflavin derivatives in black tea and catechin derivatives in green tea inhibit HIV-1 entry by targeting gp41. *Biochim Biophys Acta* 1723:270–281.
33. Ferrer M, et al. (1999) Selection of gp41-mediated HIV-1 cell entry inhibitors from biased combinatorial libraries of non-natural binding elements. *Nat Struct Biol* 6:953–960.
34. Zhou G, et al. (2000) The structure of an HIV-1 specific cell entry inhibitor in complex with the HIV-1 gp41 trimeric core. *Bioorg Med Chem* 8:2219–2227.
35. Plemper RK, et al. (2005) Design of a small-molecule entry inhibitor with activity against primary measles virus strains. *Antimicrob Agents Chemother* 49:3755–3761.
36. Plemper RK, et al. (2004) A target site for template-based design of measles virus entry inhibitors. *Proc Natl Acad Sci USA* 101:5628–5633.
37. York J, Dai D, Amberg SM, Nunberg JH (2008) pH-induced activation of arenavirus membrane fusion is antagonized by small-molecule inhibitors. *J Virol* 82: 10932–10939.
38. Bodian DL, et al. (1993) Inhibition of the fusion-inducing conformational change of influenza hemagglutinin by benzoquinones and hydroquinones. *Biochemistry* 32: 2967–2978.
39. Qi Z, et al. (2008) Rationally designed anti-HIV peptides containing multifunctional domains as molecule probes for studying the mechanisms of action of the first and second generation HIV fusion inhibitors. *J Biol Chem* 283:30376–30384.
40. Gustchina E, Bewley CA, Clore GM (2008) Sequestering of the prehairpin intermediate of gp41 by peptide N36Mut(e,g) potentiates the human immunodeficiency virus type 1 neutralizing activity of monoclonal antibodies directed against the N-terminal helical repeat of gp41. *J Virol* 82:10032–10041.
41. Bond S, et al. (2005) Polycyclic agents for the treatment of respiratory syncytial virus infections. *WO2005061513 A1*.
42. Cianci C, et al. (2004) Orally active fusion inhibitor of respiratory syncytial virus. *Antimicrob Agents Chemother* 48:413–422.
43. Dischino DD, et al. (2003) Development of a photoaffinity label for respiratory syncytial virus inhibitors. *J Labelled Comp Radiopharm* 46:1105–1116.
44. Eckert DM, Malashkevich VN, Kim PS (1998) Crystal structure of GCN4-pIQI, a trimeric coiled coil with buried polar residues. *J Mol Biol* 284:859–865.
45. Doyle J, et al. (2006) Two domains that control prefusion stability and transport competence of the measles virus fusion protein. *J Virol* 80:1524–1536.
46. Russell RJ, et al. (2008) Structure of influenza hemagglutinin in complex with an inhibitor of membrane fusion. *Proc Natl Acad Sci USA* 105:17736–17741.
47. Prussia AJ, Plemper RK, Snyder JP (2008) Measles virus entry inhibitors: A structural proposal for mechanism of action and the development of resistance. *Biochemistry* 47:13573–13583.
48. Yu K-L, et al. (2007) Respiratory syncytial virus fusion inhibitors. Part 4: Optimization for oral bioavailability. *Bioorg Med Chem Lett* 17:895–901.
49. Hallak LK, Spillmann D, Collins PL, Peeples ME (2000) Glycosaminoglycan sulfation requirements for respiratory syncytial virus infection. *J Virol* 74:10508–10513.
50. Mossessova E, Lima CD (2000) Ulp1-SUMO crystal structure and genetic analysis reveal conserved interactions and a regulatory element essential for cell growth in yeast. *Mol Cell* 5:865–876.
51. Read RJ (1986) Improved Fourier coefficients for maps using phases from partial structures with errors. *Acta Crystallogr A* 42:140–149.
52. Pinheiro JC, Bates DM (2000) *Mixed-Effects Models in S and S-PLUS* (Springer, New York), pp 528.